

CERN-TH/2002-195
 UTHEP-02-0802
 MPI-PhT-2002-036

Electric Charge Screening Effect in Single-W Production with the KoralW Monte Carlo^{*}

S. Jadach^a, W. Płaczek^{b,c}, M. Skrzypek^{a,c}, B.F.L. Ward^{d,e,c} and Z. Was^{a,c}

^a*Institute of Nuclear Physics, ul. Radzikowskiego 152, 31-342 Cracow, Poland*

^b*Institute of Computer Science, Jagellonian University,
 ul. Nawojki 11, Cracow, Poland*

^c*CERN, Theory Division, CH-1211 Geneva 23, Switzerland*

^d*Department of Physics and Astronomy,*

The University of Tennessee, Knoxville, TN 37996-1200, USA

^e*Werner-Heisenberg-Institut, Max-Planck-Institut für Physik, Föhringer Ring 6,
 80805 Munich, Germany*

Abstract

Any Monte Carlo event generator in which only initial state radiation (ISR) is implemented, or ISR is simulated independently of the final state radiation (FSR), may feature too many photons with large transverse momenta, which deform the topology of events and result in too strong an overall energy loss due to ISR. This *overproduction* of ISR photons happens in the presence of the final state particle close to the beam particle of the same electric charge. It is often said that the lack of the electric charge screening effect between ISR and FSR is responsible for the above pathology in ISR. We present an elegant approximate method of curing the above problem, without actually reinstalling FSR. The method provides theoretical predictions of modest precision: $\leq 2\%$. It is, however, sufficient for the current 1W data analysis at the LEP2 collider. Contrary to alternative methods implemented in other MC programs, our method works for the ISR multiphotons with finite p_T . Although this method is not an exact implementation of the complete/exact ISR, FSR and their interference, it is very closely modelled on it. We present a variety of numerical results obtained with the newest version of the KoralW Monte Carlo, in which this method is already implemented.

To be submitted to European Physical Journal C

* Work supported in part by the Polish Government grants KBN 5P03B09320, 2P03B00122, the NATO Grant PST.CLG.977751, the US DoE contract DE-FG05-91ER40627, the European Commission 5-th framework contract HPRN-CT-2000-00149 and the Polish-French Collaboration within IN2P3 through LAPP Annecy.

1 Introduction

In the Monte Carlo programs for e^-e^+ colliders, one has to model initial state radiation (ISR) as precisely as possible. For some processes where the precision requirements are moderate, such as the single- W production process at LEP, where the combined LEP2 precision is estimated at $\sim 7\%$, see Ref. [1], it is sufficient to implement ISR in the leading-logarithmic (LL) approximation. This can be done by modelling ISR in the collinear, $p_T = 0$, approximation (see for instance refs. [2,3]), by “unfolding” the strictly collinear structure functions [4] or using the so-called “parton shower” technique as in Ref. [5] (recently employed also in [6]), or the Yennie–Frautschi–Suura (YFS) exclusive exponentiation employed in Ref. [7]; see Ref. [8] for a more complete list of references. In all of the above MC programs the final state radiation (FSR) from charged final particles is either not modelled at all or simulated completely independently of the ISR, which is the general spirit of the LL approximation. This may be problematic if one of the final state charged particles gets close to the beam particle with the same electric charge. In such a case ISR photon emission is damped, because of the well-known *electric charge screening* effect (ECS), and the total energy distribution of the ISR photons gets softer. In the terminology of the LL it is described as the “decrease of the LL scale” from s , which is the square of the centre-of-mass-system (CMS) energy, to t , which is the four-momentum transfer (squared) from the beam to the nearby particle of the same charge. We shall refer to the above phenomenon as the *leading-logarithmic scale transmutation* (LLST).

Let us stress that in the calculations based from the beginning on the YFS exclusive exponentiation, as in the BHWIDE [9] or KKMC [10,11] MC programs, the ECS and LLST are automatically built in to an infinite order, hence there is no need to re-install them. The ECS and LLST in exclusive exponentiation are direct manifestations of the interference effects between ISR and FSR. Hence, they are also often described as “coherence effects”.

As already said, owing to the lack of ECS in the Monte Carlo calculation in which ISR is modelled using the s -scale, one may encounter two pathologies: (a) overproduction of photons with large transverse momenta, which results in the noticeable deformation of the topology of events and (b) too strong an overall energy loss due to ISR. In particular this happens in the single- W ($1W$) production process at LEP2, when modelled by the MC program KoralW [12,13,14]. The aim of this work is to invent a simple method of correcting for ECS, and curing the above deficiencies, without the need of generating FSR in the MC¹. The method is quite general, although its most immediate application is improving the theoretical prediction for the $1W$ production process at LEP2 to the $\leq 2\%$ precision level. Contrary to alternative curing methods implemented in the other MC programs [3,5], our method works for finite- p_T ISR multiphoton distributions. It is not an “ad hoc” method because its development is based on the consideration of the exact

¹An obviously better alternative is to implement YFS exclusive exponentiation for the entire $e^-e^+ \rightarrow 4f$ process. This is however too much work to be completed before the end of the LEP2 data analysis. For the $e^-e^+ \rightarrow WW \rightarrow 4f$ subprocess, where precision requirements are $\sim 0.5\%$, the ECS/coherence effects between ISR and FSR (W decays) are strongly suppressed.

YFS exclusive exponentiation for ISR, FSR and their interference [11].

After defining our method, we shall also present a variety of numerical results exploiting the newest version of the KoralW Monte Carlo, in which this method of introducing ECS is already implemented.

The *electric charge screening* effect together with *leading-logarithmic scale transmutation* for the multiphoton emission are described in the following section. The proposed method is *practical* because:

- the effects are introduced by means of a simple well-behaving Monte Carlo weight,
- it does not require generation of the additional photons in the final state (FSR),
- it provides an ISR precision good enough for LEP2 data analysis, that is $\leq 2\%$.

The construction of the ECS weight is first described in Section 1.2, using a simple example of the process $\mu^-\mu^+ \rightarrow \mu^-\mu^+$, for which the ECS effect and the method of its introduction in the ISR is illustrated with the help of many examples of the photon distributions. This method is later generalized to the $e^-e^+ \rightarrow 4f$ process in Section 2, where also the relevant correction to the virtual form factor (overall normalization) is defined. Numerical cross-checks and final discussion are provided in Section 4.

1.1 Electric charge screening

The electric charge screening effect is a well-known phenomenon of suppression of the photon emission from any subset of compensating charges (charges adding to zero or to small total charge), which are close in the momentum phase space, i.e. which have small effective mass, small angular distance, etc. One should exclude from the consideration charges/particles that are well *time-separated*, i.e. from the decay and production parts of the narrow resonance production/decay processes. A good example of a subset of compensating charges is for instance a fast-moving light $\mu^+\mu^-$ pair – a “dipole” of compensating charges. For the compensation considerations, electric charges of every initial state particle should be assigned an additional minus sign with respect to particle charges in the final state (much as in the definition of the four-momentum transfer). For instance in the low-angle Bhabha (LABH) process, the initial state e_i^- and the final state e_f^- form together a “dipole” of compensating charges and the ECS/LLST takes place, which means that the emission of photons with an angle greater than the angular size of the (e_i^-, e_f^-) compensating system gets strongly suppressed.

The leading-logarithmic scale transmutation is just another face of the same ECS. For ISR taken alone, the LL parameter $L_e(s) = 2\frac{\alpha}{\pi} \ln \frac{s}{m_e^2}$, which controls the strength of the loss of the total energy due to ISR, is defined for the so-called LL energy scale \sqrt{s} , being just the total centre-of-mass system (CMS) energy. Actually this so-called big logarithm $L_e(s)$ comes from the integral over the photon angle $L_e(s) \simeq \int_{m^2/s}^{\pi} \frac{d\theta}{\theta}$. Taking into account the interference between ISR and FSR introduces ECS. This becomes important when, for instance, one of the final state e^- 's approaches the initial beam e^- by an angle θ .

Then, the photon angular distribution gets suppressed (i.e. loses the $1/\vartheta$ dependence) for $\vartheta > \theta$. Hence $L_e(s)$ gets replaced in the so-called LL ISR structure functions by a smaller $L_e(t) \simeq \int_{m^2/s}^{|t|/s} \frac{d\vartheta}{\vartheta}$. Obviously, LLST is a numerically important effect when $|t| \ll s$. Such is the case of the $1W$ production, where at least one of the final state electrons gets inside the beam pipe due to the strong peak in its scattering angle (because of t -channel photon exchange in the Born distribution).

All the above discussion was for real photons, and in fact the whole ECS can be viewed as an almost completely *classical* phenomenon. The real photon angular distribution, in the soft-limit approximation, is just the square of the classical electric current vector. Quantum-mechanical virtual corrections merely correct the overall normalization, cancelling properly infrared (IR) singularities in the photon *energy* distribution. (The IR-divergent part of the exponentiated virtual correction has necessarily $L_e(t)$ as a coefficient.)

1.2 “Mhamha” toy example

As already indicated, in our method of implementing the ECS effect in ISR we do not include explicit FSR; however, we take as a guide the YFS model in which ISR, FSR and their interference are included. In this section we examine carefully the ECS effect for a single real photon in such a complete model, proposing at the end of the exercise a simple correcting weight introducing the ECS effect in the pure ISR case.

The above will be done by carefully scrutinizing several variants of the angular photon distributions of a “toy process”:

$$\mu^-(p_a) + \mu^+(p_b) \rightarrow \mu^-(p_c) + \mu^+(p_d) + \gamma(k), \quad (1)$$

a muonic analogue of the Bhabha process, which we shall call a “Mhamha scattering process”². In the soft photon limit, the final state distribution is equal to the Born distribution times the *complete* soft photon factor

$$\tilde{S}_{abcd} = -\frac{\alpha}{4\pi^2} \left(\frac{p_a}{kp_a} - \frac{p_b}{kp_b} - \frac{p_c}{kp_c} + \frac{p_d}{kp_d} \right)^2, \quad (2)$$

the same factor which is a basic element in the YFS exponentiation [15]. In order to see the ECS effect we compare the above complete \tilde{S}_{abcd} with the incoherent sum $\tilde{S}_{ab} + \tilde{S}_{cd}$ of the ISR and FSR contributions, neglecting the interference $\text{IFI} = \text{ISR} \otimes \text{FSR}$, where

$$\tilde{S}_{ab} = -\frac{\alpha}{4\pi^2} \left(\frac{p_a}{kp_a} - \frac{p_b}{kp_b} \right)^2, \quad \tilde{S}_{cd} = -\frac{\alpha}{4\pi^2} \left(\frac{p_c}{kp_c} - \frac{p_d}{kp_d} \right)^2. \quad (3)$$

We choose a relatively small scattering angle θ_{ab} . In Fig. 1 we plot $\tilde{S}_{ab} + \tilde{S}_{cd}$ and complete \tilde{S}_{abcd} side by side, as a function of the photon polar variables $(\cos \vartheta, \varphi)$. In order to see very clearly the structure of the distribution over the entire unit sphere, we choose $(\cos \vartheta, \varphi)$

²The name “Mhamha” was suggested by A. Blondel in the context of the muon collider studies.

with respect to the z -axis pointing perpendicularly to the beam axis (beams are along the x -axis). We choose $\sqrt{s} = 5$ GeV at which muons are already very relativistic and the muon scattering angle 20° – small enough to see ECS effect. The four peaks of the photon emission intensity in Fig. 1 are centred around directions of the four charged muons. The ECS effect is seen as a clear suppression of the photon emission intensity beyond the two dipole peaks (a, c) and (b, d) . The first dipole is for the incoming and outgoing μ^- and the second one is for the incoming and outgoing μ^+ . In Fig. 1 the two t -channel dipole peaks are much sharper for the complete \tilde{S}_{abcd} than for the incoherent superposition of ISR and FSR, $\tilde{S}_{ab} + \tilde{S}_{cd}$. The top part of the dipole peaks is worth inspection, see Fig. 2, as it features the well-known “helicity zeros” as deep “craters”, exactly in the direction of the emitter charge. The craters are of an angular size m_μ/E_{beam} and will shrink to a negligible size at very high energies. The ECS effect is also very clearly seen again in Fig. 2, as a strong sharpening of the photon radiation intensity beyond the dipole double peak.

Is the radiation pattern of \tilde{S}_{abcd} , which we see in Fig. 2, specific to a t -channel character of the process? Not really. The radiation pattern of the real $\mu^- \mu^+$ pair with effective mass equal to $\sqrt{|t|}$ and boosted to the total energy of 5 GeV is completely *undistinguishable* from what we see in Fig. 2. The other way of describing it is that \tilde{S}_{abcd} is extremely well approximated by the incoherent sum of $\tilde{S}_{ac} + \tilde{S}_{bd}$. Let us stress that \tilde{S}_{ac} and \tilde{S}_{bd} look very simple and natural in the two Breit frames (rest frames of (a, c) and (b, d)) and the *non-trivial* shape of the photon intensity in Fig. 2 is the result of the *trivial* Lorentz boost from the Breit to the CMS frame. (In a sense, the non-trivial shape plotted in Fig. 2 is the “fault” of the observer himself, who has chosen to examine it from an “unnatural” reference frame.) The other interesting observation is that if we have plotted $\tilde{S}_{ac} + \tilde{S}_{bd}$ in Figs. 1 and 2 then we will have found that it is completely undistinguishable from the \tilde{S}_{abcd} ³. In order to see any noticeable difference between these two distributions, we have to go to the backward scattering angle. We do this in Fig. 3, where we compare these two emission distributions for the scattering angle $\theta = 135^\circ$. The peaking structure is the same; however, for \tilde{S}_{abcd} we see a rich interference pattern, especially for photons far away from the four charges. At this large scattering angle we have checked that the $\tilde{S}_{ac} + \tilde{S}_{bd}$ and $\tilde{S}_{ab} + \tilde{S}_{cd}$ distributions look almost identical.

1.3 ECS weight – preliminaries

Having seen in Figs. 1 and 2 what the coherence ECS effect is, let us now ask the important practical question: Provided that, as in KoralW, we have only ISR, could we modify the ISR distribution in such a way that we get the same sharpening of the photon angular distribution, as in the real world of the coherent \tilde{S}_{abcd} ? Our proposal for the correcting weight is the following:

$$W_{\text{ECS}}(k) = \frac{\tilde{S}_{abcd}(k)}{\tilde{S}_{ab}(k) + \tilde{S}_{cd}(k)}, \quad (4)$$

³This is why the BHWIDE MC program, which models $\tilde{S}_{ac} + \tilde{S}_{bd}$ at the low MC level, is so efficient in modelling the multiphoton radiation in the complete wide-angle Bhabha process.

and we are going to show that it does what we want. Let us examine the corrected ISR distribution

$$\tilde{S}_{ab}(k)W_{\text{ECS}}(k). \quad (5)$$

First, we notice that $W_{\text{ECS}}(k) \simeq 1$ (apart from the unimportant helicity zero) close to the angular position of the outgoing particles, so it does not try to re-install the FSR, and the corresponding MC weight should not have an inconvenient long tail. Then, what is most important, W_{ECS} really cuts off very strongly photon emission at angles greater than the scattering angle θ_{ac} or θ_{bd} . This is seen very clearly in Fig. 4, where the “angular size” of the corrected ISR emission pattern shrinks by a factor of ~ 3 with respect to the original one. This is clearly visible even for our moderately small scattering angle $\theta_{ac} = 20^\circ$. In the real KoralW application we shall, of course, apply the product of the $W_{\text{ECS}}(k)$ over all ISR photons. The overall normalization will also be corrected by means of correcting the exponential virtual+real form factor, which also compensates for the IR divergence of the average ECS weight $\langle \prod_i W_{\text{ECS}}(k_i) \rangle$.

How does one justify the fact that we apply a correcting weight, which includes ISR \otimes FSR interference, without generating FSR in the MC? A quite general answer is that the above can be understood as a procedure of integrating analytically over the real FSR photons and including the result of the integration in the normalization⁴. Such a procedure can be very close to experimental reality, provided the FSR photons are combined with the outgoing charged particles. From the theoretical point of view the above procedure is quite common in the world of the LL approximation. For example, a similar solution is used to install interference between different branches of FSR in the PHOTOS Monte Carlo [16]. As we shall see later on, our procedure not only makes sense in the LL approximation, but also features the precise IR cancellations and has the expected LL behaviour.

2 ECS Correction weight for the $4f$ process

We have already explained what the ECS effect is, and sketched how to introduce it in an approximate way in the ISR Monte Carlo, with the help of the correcting weight W_{ECS} . All that was done for the $2f$ final state in a rather *qualitative* way. In the following we define the analogous correcting procedure for the four-fermion ($4f$) final state; we shall also present several *quantitative* tests, see Section 4.

2.1 Real emission part of W_{ECS}

Let us start by defining the real emission part of the W_{ECS} for the $4f$ process $e^-e^+ \rightarrow f_c(p_c) + \bar{f}_d(p_d) + f_e(p_e) + \bar{f}_f(p_f)$. For this process the complete soft photon emission factor

⁴The FSR photons can be added later on; however, care must be taken to get the ECS for the FSR in a similar way as for ISR.

reads

$$\tilde{S}(k) = \frac{1}{2} \sum_{\substack{i,j=a,b,\dots,f \\ i \neq j}} \tilde{S}_{ij}(k), \quad \tilde{S}_{ij}(k) = Z_{ij} \frac{\alpha}{4\pi^2} \left(\frac{p_i}{kp_i} - \frac{p_j}{kp_j} \right)^2, \quad (6)$$

where $Z_{ij} = Z_i Z_j \theta_i \theta_j$, Z_i is the sign of the i -th charge, and $\theta_i = +(-)$ if particle i is outgoing (incoming). The natural extension of the weight of Eq. (4) would be

$$W_{\text{ECS}}^{\text{real}} = \frac{\tilde{S}(k)}{\tilde{S}_{ab}(k) + \tilde{S}_{cdef}(k)}, \quad (7)$$

where \tilde{S}_{cdef} is defined as in Eq. (6), restricting summation to the FSR part, $i, j = c, d, e, f$. The above weight could be implemented in the MC without much problem; however, it would complicate the construction of the accompanying normalization weight $W_{\text{ECS}}^{\text{norm}}$ described in the next section.

We have noticed, however, that since we are working in the LL framework, we can simplify the weight of Eq. (7), and effectively replace it with the variant of the $2f$ weight of Eq. (4). How is this possible? One has to keep in mind that our aim is to deal with the situation in which one of the final state particles (electrons) is close to the beam or two particles (electrons/positrons) are close to the beams. Let us call the above two situations (following a long established terminology) singly- and doubly-peripheral scattering.

In the singly-peripheral (SP) situation we expect ECS in only one hemisphere. Photons will be emitted inside a narrowly collimated t -channel dipole close to the beam; there will be a *gap in the photon angular distribution* extending from the dipole down to the nearest particle in the “central region”⁵ out of the remaining three final particles. In the doubly-peripheral (DP) configuration, we shall have two narrowly collimated t -channel dipoles close to the beams and two gaps down to the central region. In fact the two gaps will join together in the central region. This gap structure will be clearly seen in the numerical results in Section 4, where we shall plot the photon distribution in the rapidity variable $y = -\ln \tan(\vartheta_\gamma/2)$.

Now, if our main aim is to reproduce one or two of the ECS gaps in ISR radiation, and if we restrict ourselves to the LL approximation, then it does not matter how many particles there are in the central region. What *really* matters is how many (one for SP and two for DP case) particles close to the beams there are, and at which angles those closest to the beams (members of t -channel dipoles) are. Consequently, in the LL approximation, for the purpose of reproducing ECS, it is perfectly safe to replace the four final particles by just two (especially that there are only two beams). In the DP case, the choice is clear: we take those two particles closest to the beams and properly match the beam charges (form together with the beams t -channel dipoles), ignoring the other two (charge conservation is of course respected). In the SP case one charge is again the member of the t -channel dipole and another charge we place anywhere in the central regions; it may be tied up with one of the three remaining particles or not – it does not matter.

⁵By central region we understand angles greater than, say, 10° from both beams.

The two final “effective final state particles” entering the ECS weight we shall denote C and D , and the real-emission part of our ECS weight we define as follows

$$W_{\text{ECS}}^{\text{real}} = \prod_i w^R(k_i), \quad w^R(k) = \frac{\tilde{S}_{ab}(k) + \tilde{S}_{CD}(k) + \tilde{S}_{aC}(k) + \tilde{S}_{bD}(k) + \tilde{S}_{aD}(k) + \tilde{S}_{bC}(k)}{\tilde{S}_{ab}(k) + \tilde{S}_{CD}(k)}. \quad (8)$$

The above formula, apart from notation, is identical to that of Eq. (4). Also, in the numerator we have used the algebraic identity of Ref. [15] in order to decompose \tilde{S}_{abCD} into six dipole-type contributions.

In practice, the final state fermions C and D in Eq. (8) are determined by the kinematics of the final state (FS). In the case of the so-called “single- W ” ($1W$) final state, in which we are mainly interested here, we check whether one final state electron (positron) is lost in the beam pipe and the decay products of the $1W$ are visible outside the beam pipe. In such a case we identify the in-beam-pipe particle as one of the effective particles C or D (according to its charge). As for the other one, there is freedom of its choice, as explained above. Since all other FS fermions are at large angles (central region) it should not matter which one we pick. In fact we do something even more primitive: we assign the second remaining C or D as directed perpendicularly to the beam pipe. In the second, DP case of the $e^-e^+f\bar{f}$ final state with both e^-e^+ lost in the beam pipe, we assign C and D to e^- and e^+ , of course.

Let us summarize the main points on the weight of Eq. (8), as implemented in KoralW:

- The only purpose of the weight $W_{\text{ECS}}^{\text{real}}$ is to restore the ECS effect due to $\text{ISR} \otimes \text{FSR}$ interference.
- We do not aim at re-creating the FSR. This would be formally possible with a similar weight; however, it would lead to an awful weight distribution and a non-convergent MC calculation.
- We get $W_{\text{ECS}}^{\text{real}} \rightarrow 1$ for photons collinear with the FS effective fermions C and D . This ensures a very good weight distribution.
- The FSR can be treated separately, either inclusively (calorimetric acceptance) or exclusively, generated with the help of PHOTOS⁶.

Finally, we notice that in the ECS weight we may insert massless four-momenta without any problem – in practice we shall use a massless limit of Eq. (6):

$$\tilde{S}_{ij}(k) \rightarrow \tilde{S}_{ij}(k) = Z_{ij} \frac{\alpha}{4\pi^2} \frac{-2p_i p_j}{(kp_i)(kp_j)}. \quad (9)$$

⁶Care has to be taken to implement ECS for FSR, if necessary.

2.2 Virtual+soft correction to normalization

The average of the real emission weight $\langle W_{\text{ECS}}^{\text{real}} \rangle$ taken alone is infrared (IR)-divergent as $\sim \ln \epsilon$, where ϵ defines the infrared cut $E_\gamma > \epsilon E_{\text{beam}}$ on the photon momentum in the CMS. In the YFS exponentiation of ISR in KoralW, based on Ref. [17], the IR cancellations occur *numerically* between the real soft-photon factors $\prod_i \tilde{S}(k_i)$ and the YFS form factor $F_{\text{YFS}} = \exp(2\alpha B + \tilde{B}(\epsilon))$ (contrary to typical parton-shower MCs, where they are built-in features of the MC algorithm). Since it is well known how these IR cancellations do occur, see refs. [17, 11], it is therefore also possible to calculate the IR violation of the $\langle W_{\text{ECS}}^{\text{real}} \rangle$, and to correct for the above divergence *precisely*. At the same time, we shall also correct for the LLST in the virtual part of the YFS form factor and the non-infrared LL corrections to the $\mathcal{O}(\alpha)$. As a result, the corrected total cross section will become again independent of the IR parameter ϵ , as the original one. This we shall check numerically. Again, all of this procedure should be regarded as a “shortcut” with respect to the full YFS exponentiation with ISR+FSR including ISR \otimes FSR interference, keeping in mind that our precision tag is limited to 2%, and that simplicity of the method is also our high priority.

The correction to the overall normalization, which corrects for the IR divergence exactly, and introduces LLST in the virtual LL correction, reads as follows:

$$W_{\text{ECS}}^{\text{norm}} = \exp\left(\frac{3}{4}(\bar{\gamma}_t - \gamma_s)\right) \exp(\Delta U(\epsilon))$$

$$\Delta U(\epsilon) = U(\epsilon) - U_R(\epsilon), \quad U(\epsilon) = \int_{\epsilon\sqrt{s}/2}^{\sqrt{s}} \frac{d^3k}{k^0} \tilde{S}_{ab}(k), \quad U_R(\epsilon) = \int_{\epsilon\sqrt{s}/2}^{\sqrt{s}} \frac{d^3k}{k^0} \tilde{S}_{ab}(k) w^R(k). \quad (10)$$

The factor $\exp(\Delta U)$ cancels *exactly* the ϵ -dependence and compensates *approximately* for the normalization change due to the $\langle W_{\text{ECS}}^{\text{real}} \rangle$ weight. The proof and details of construction of $\exp(\Delta U)$ are given in Appendix A.

The factor $\exp((3/4)(\bar{\gamma}_t - \gamma_s))$ provides the LLST in the virtual part of the form factor. The γ_s is defined as $\gamma_s = 2(\alpha/\pi)(\log(s/m_e^2) - 1)$. The scale of the $\bar{\gamma}_t$ depends on the number of final state particles that effectively contribute to the interference weight (8). When only one line is modified, say e^- , we have $\bar{\gamma}_t = (1/2)(\gamma_s + \gamma_{t^-})$, where $\gamma_{t^-} = 2(\alpha/\pi)(\log(|t^-|/m_e^2) - 1)$ and t^- denotes the square of the four-momentum transfer from the e^- line. When both e^- and e^+ lines are modified, we get $\bar{\gamma}_t = (1/2)(\gamma_{t^-} + \gamma_{t^+})$.

The triple integral of Eq. (10) has to be computed for every generated event. It is therefore of high importance to be able to do it very fast, so that the Monte Carlo generation is not slowed down too much. We have not attempted to compute it completely in an analytic way. Instead, we perform two out of three integrations analytically and the remaining one numerically. Such a procedure proved to be fast enough. We show in Appendix B how to reduce the integral in Eq. (10) to a simple one-dimensional integral.

3 Running QED Coupling Constant

In the practical applications, a more precise prediction for the $1W$ -type processes requires also the inclusion of the effect of the running QED coupling constant in the e^- (e^+) vertex from the value at M_W^2 scale to the actual small transfer value t^- (t^+). We include this effect in the form of an overall factor that multiplies the whole matrix element squared. It is activated only for the electron or positron line (in the Feynman diagram) for which the ECS corrective weight is actually applied. In the SP case of one e^\pm line, the correcting weight reads:

$$W_{Run} = W_{Run}^\pm = \left(\frac{\alpha(t^\pm)}{\alpha_{G_\mu}} \right)^2, \quad (11)$$

where α_{G_μ} is the value of coupling constant in the G_μ scheme⁷. For the DP case (two lines) we put

$$W_{Run} = W_{Run}^- W_{Run}^+. \quad (12)$$

The precision of such a naive solution is, in most cases (including leptonic final states), better than 2%, and for semileptonic final states even better than 1%, as discussed at length in Ref. [18].

4 Numerical results

In this section we check very carefully that our ECS weight

$$W_{ECS} = W_{ECS}^{norm} W_{ECS}^{real} W_{Run} \quad (13)$$

introduces the ECS effects in the photon angular distribution, the LLST in the total energy loss due to ISR photons, and corrects the QED coupling constant for the hard process.

4.1 General consistency tests

In this subsection we present some numerical results that demonstrate the action of the weight emulating the ECS effect.

The first test, necessary for consistency, shows that the cross-section is independent of the dummy IR cut-off ϵ of Eq. (10). In Table 1 we show the values of the total cross sections for the $e\bar{\nu}_e u\bar{d}$ channel for a few values of the dummy IR cut-off ϵ . The energy is set to 190 GeV, and the cut-off on the maximal angle of the scattered electron is 2.5° w.r.t. the electron beam in the effective CMS frame of outgoing particles. One can see that, within the statistical errors, there is indeed no dependence on the ϵ .

Having checked the self-consistency of the emulation, we can now proceed to demonstrate the main result of this work – the ECS suppression of the transverse radiation. In

⁷ If any scheme other than G_μ is used in KoralW, the program will report a conflict and stop at this point.

ϵ	10^{-3}	10^{-4}	10^{-5}	10^{-6}	10^{-8}	10^{-9}	10^{-10}
σ	0.09773	0.09757	0.09755	0.09752	0.09762	0.09737	0.09759
[pb]	± 0.00020	± 0.00022	± 0.00010	± 0.00019	± 0.00019	± 0.00020	± 0.00011

Table 1: Value of the total cross section for the $e\bar{\nu}_e u\bar{d}$ final state, for various values of the dummy IR cut-off ϵ_{IR} .

Fig. 5 we show (in the doubly-logarithmic scale) the differential distributions $d\sigma/dy$ with (red dots) and without (blue open squares) the correction weight for the ECS effect for the $e^+e^-s\bar{s}$ channel. The angles of scattered electron and positron are set to be between 2 and 0.2° w.r.t. the beam line (the double “ice-cream-cone” configuration around the beam line) in the laboratory frame. The distribution is obtained by summing over *all* photons of a given event and is normalized to arbitrary units. The $y = -\log_{10} \tan(\theta_\gamma/2)$ is proportional to the (pseudo)rapidity of the photon.

The scattering cone of electron (positron) corresponds, in the y scale, to the values from 1.76 to 2.76 (-1.76 to -2.76) and are marked in the plot with blue shadow bands. In the Figure one can clearly see the ECS suppression between these bands. The spectrum for photon emission outside the area (i.e. inside the e^- and e^+ cones) remains flat and unchanged. Between the bands (i.e. outside the e^- and e^+ cones) the suppression is clearly visible. We have fitted the suppressed spectrum with straight lines. The values of the fitted slopes are shown in the figure to be in good agreement with the values of ± 2 , which means that we see the $1/\theta_\gamma^2$ suppression of the photons beyond the dipole angular size, naively expected from the “multipole expansion”.

In the next step we look into the $1W$ -type final state of $e\bar{\nu}_e u\bar{d}$. This time, there is only one electron in the final state, so we expect the suppression area to be asymmetric – only in the forward direction. The result of the simulation is shown in Fig. 6. In blue (open squares) we show the same curve as in Fig. 5, i.e. the $e^-e^+s\bar{s}$ case (appropriately renormalized), whereas in red (dots) we present the new $e\bar{\nu}_e u\bar{d}$ result. Shadowed bands again visualize the location of the electron (positron) “ice-cream-cones”. For the $e\bar{\nu}_e u\bar{d}$ case the area corresponds to the “ice-cream-cone” between 0.2 and 0.5° . The other end of the $e\bar{\nu}_e u\bar{d}$ suppression area is located at zero (90°), where the fictitious particle is located and leaves the radiation in the backward hemisphere unchanged. Note that the exact location of this fictitious particle (in the area of reasonably large angles) is irrelevant anyway, as the effect depends on it logarithmically. The fitted lines can be used as before to confirm the correctness of the suppression factor (slope).

Finally, in Fig. 7 we show the $e\bar{\nu}_e u\bar{d}$ process for two different values of the half-opening angle of the electron “ice-cream-cones”: 0.2 to 0.5° and 0.02 to 0.05° . One can see that the left (backward) edge of the suppression area is, as expected, identical in the two cases, whereas the right (forward) edge follows the electron opening angle (the range of this angle is marked with shadowed bands).

Another characteristic distribution is the $d\sigma/d\log_{10} v$ distribution, with the definition $v = 1 - s'/s$. As this distribution is sensitive only to the value of the transfer in the hard scattering process, we have defined the acceptance cuts for this exercise to be $-9 >$

$\log(t/s) > -11$. In the limit of small v (soft limit) we know from YFS exponentiation that⁸ $d\sigma/dv = \exp(3/4\gamma)F(\gamma)\gamma v^{\gamma-1}\sigma((1-v)s)$ where $F(\gamma) = \exp(-\gamma C_{Euler})/\Gamma(1+\gamma) = 1 + \mathcal{O}(\gamma^2)$. The γ for the case of pure s -channel ISR is governed by the scale s , i.e. $\gamma_s = 2\alpha/\pi(\log(s/m_e^2) - 1)$. Inclusion of the ECS suppression leads to the replacement of the scale $s \rightarrow |t|$, i.e. $\gamma_t = 2\alpha/\pi(\log(|t|/m_e^2) - 1)$. In the case of the $1W$ -type process ($e\bar{\nu}_e u\bar{d}$) this suppression happens only in the electron line, whereas for the positron line we still retain the scale s , so the effective $\bar{\gamma}_t$ becomes $\bar{\gamma}_t = 1/2(\gamma_s + \gamma_t)$. For the e^+e^- case, the suppression happens for both lines and we have $\bar{\gamma}_t = \gamma_t$.

In Fig. 8, we show a ratio of $d\sigma/d\log_{10} v$ distributions with and without the ECS correction for the processes $e^+e^-s\bar{s}$ (blue open squares) and for $e\bar{\nu}_e u\bar{d}$ (red dots). For the $e^+e^-s\bar{s}$ process we applied an additional cut-off of 3.5 mrad for the minimal angle of s and \bar{s} quarks with respect to the beam line and we used the so-called ‘‘extrapolation procedure’’ that preserves the value of smallest transfer (see KoralW manual [7] for details). As follows from the above discussion, we expect to see (in doubly-logarithmic scale) straight lines of the form $a + b\log_{10}(v)$ where the slope of the line should hence be given by $b_{th} = \bar{\gamma}_t - \gamma_s = \alpha/\pi\log(t/s)$ and the free coefficient by $a_{th} = 3/4(\bar{\gamma}_t - \gamma_s)\log_{10}(e) + \log_{10}(\bar{\gamma}_t/\gamma_s)$. In our exercise the average value of the $\log(t/s)$ as calculated in the simulation is $\log(t_0/s) = -9.86$. This leads, at $t = t_0$, to the expected theoretical values of slopes of $b_{th} = -0.023$ and $a_{th} = -0.104$ for $e\bar{\nu}_e u\bar{d}$ and $b_{th} = -0.046$ and $a_{th} = -0.241$ for $e^+e^-s\bar{s}$. The corresponding results of the fits of the actual Monte Carlo simulations to straight lines, shown in the insets in Fig. 8, are $b_{th} = -0.021 \pm 0.002$ and $a_{th} = -0.093 \pm 0.005$ for $e\bar{\nu}_e u\bar{d}$ and $b_{th} = -0.049 \pm 0.003$ and $a_{th} = -0.24 \pm 0.01$ for $e^+e^-s\bar{s}$. We see an agreement at the level of one standard deviation for the e^+e^- case and two standard deviations for the case of one electron. The latter discrepancy can be a signal that our naive expectation for the slope is good only to a few per cent of its value. The value of the free coefficient is in principle sensitive to the overall normalization factor (3/4). It is however numerically dominated by a much larger $\log_{10}(\bar{\gamma}_t/\gamma_s)$ term; the actual factor of 3/4 contributes below 10%, i.e. at the level of accuracy of the whole comparison, and is, therefore, inconclusive.

4.2 Predictions for the $1W$ process

In this subsection we present a few results of the influence of the ECS effect in KoralW on the $1W$ -type process $e^+e^- \rightarrow e^-\bar{\nu}_e u\bar{d}$. We use the following cut-offs (similar to Ref. [8]):

- electron angular acceptance: $\cos\theta_e \geq 0.997$,
- quark–antiquark invariant mass: $M_{q\bar{q}} \geq 45$ GeV,

and the following setup: G_μ scheme; fixed W and Z widths; normal (non-screened) Coulomb correction; naive QCD correction; extrapolation procedure that fixes the smallest transfer (KeyISR=3); W branching ratios with mixing and naive QCD correction cal-

⁸ The YFS exponentiation alone leads only to the $\exp(\gamma/4)$ factor. The additional $\exp(\gamma/2)$ comes from leading-logarithmic considerations. In the YFS scheme this factor is supplied order by order by perturbative non-infrared corrections.

culated in IBA from the CKM matrix [19]; $G_\mu = 1.16639 \times 10^{-5}$, $M_Z = 91.1882$ GeV, $M_W = 80.419$ GeV, $\Gamma_Z = 2.4952$ GeV, $\alpha_S = 0.1185$.

E [GeV]	σ^{C+R} [fb]	$1 - \sigma^R/\sigma^{C+R}$ [%]	$1 - \sigma^C/\sigma^{C+R}$ [%]	$1 - \sigma/\sigma^{C+R}$ [%]
190	87.11 ± 0.22	5.65 ± 0.15	-5.16 ± 0.02	0.81 ± 0.14
200	103.60 ± 0.26	5.49 ± 0.15	-5.13 ± 0.02	0.67 ± 0.15
500	807.56 ± 2.74	4.92 ± 0.21	-4.68 ± 0.02	0.51 ± 0.21

Table 2: The total cross-section with ECS effect (C) and running QED coupling (R). The cut-offs and parameter setup are as described in the text. The relative size for the ECS effect and the running QED coupling effect are also shown.

In Table 2 we present the values of cross sections with the ECS effect (marked with C) and running of the QED coupling (marked with R) for a few energies in the LEP2 and future LC energy range. In the respective columns we show separately the changes due to the ECS effect (third col.), the running of the QED coupling (fourth col.) and both corrections together (fifth col.). All changes are given in per cent with respect to the corrected cross section. One can see that the reduction of ISR due to ECS suppression increases the cross section for all energies, consistently with the overall effect of ISR. The running of the QED coupling decreases the cross section by roughly the same amount regardless of the energy. The relative shifts for LEP2 energies presented in Table 2 are in a qualitative agreement with the results of Ref. [3].

4.3 Precision of the $1W$ cross sections

Finally, we have to address the question of the physical precision of the above $1W$ cross sections. There are two components of the error – approximations in the ECS treatment and approximations related to the running QED coupling and higher order EW effects.

- The approximations in the treatment of ECS are of the genuine non-leading type, i.e. α/π with possible enhancement factors (e.g. π^2). Therefore we estimate this error to be below 2%.
- Following Ref. [18], we estimate the approximation due to the naive treatment of running the QED coupling to be at most 2%, dominated by the leptonic channel contribution. In some specific cases, such as the semileptonic final states, this error can be lowered to 1% (see [18] for details).
- The other missing EW effects we estimate at 1%, again following Ref. [18].

To summarize, in the new version 1.53 of KoralW, upon adding the above contributions in quadrature, we obtain an overall precision tag of the single- W cross sections of 3%. This number can be reduced for some specific final state configurations, because of a smaller error contribution from the running QED coupling. The precision of the ECS implementation alone is of the order of 2%. Such overall theoretical precision of 3% for

the single- W cross sections lies well below the expected final LEP2 experimental accuracy of $\sim 7\%$ [1].

5 Summary

We have shown that it is possible to improve the standard ISR calculation in such a way that it takes into account electric charge screening and LL scale transformation for singly- and doubly-peripheral configuration in the production of the $4f$ final states, with electron and/or positron in the beam pipe. This is done using a relatively simple and well-behaving MC weight. The method does not necessitate an explicit inclusion of the FSR. Although the method is not the exact implementation of the YFS exclusive exponentiation for the ISR+FSR, it is nevertheless closely modelled upon it. The QED running coupling constant for the hard process is corrected at the same time to the correct t -channel scale. We also present a number of numerical consistency checks and a sample prediction for the $1W$ total cross section. The MC program KoralW (in its new version 1.53) in which this method is implemented is readily available for any interested user. It will be especially useful for the final LEP2 data analysis.

Acknowledgements

We would like to thank A. Valassi for stimulating discussions. We warmly acknowledge the kind support of the CERN TH and EP divisions.

A Virtual+soft normalization weight

In this appendix we discuss the construction of the *ad hoc* normalization weight of Eq. (10) and show that it ensures independence of the cross section from the dummy infrared cut-off ϵ .

Before going into details, let us stress again that we introduced the ECS ansatz *by hand* into the pure ISR-type MC algorithm in order to cure some low-angle-emission pathologies. Therefore it is *not* the purpose of this appendix to rigorously derive the ECS ansatz from “basic principles”. Such a rigorous introduction of the ECS requires an entire reformulation of the MC algorithm, from ISR-type to $\text{ISR}\otimes\text{FSR}$ -type, based on the complete YFS theory and has already been done in other MC programs, such as BHWIDE [9] or KKMC [10, 11].

We will use the Mellin transform representation of the MC master formula as given in Appendix A of Ref. [17]. In order to establish the notation, we will, following Ref. [17], briefly recall the relation of this representation to the standard Monte Carlo form of refs. [12, 14, 7]. Next we will show how the real emission weight is added into the master formula and what the matching virtual+soft compensation weight must look like to cancel the fictitious ϵ dependence.

We start from the Mellin transform representation of the master formula as given in Eq. (A1) of Ref. [17] adapted to the four-body final state (for details we refer to Ref. [17])

$$\begin{aligned}
\sigma = & \int \frac{d^4x}{(2\pi)^4} \int \prod_{i=1}^4 \frac{d^3q_i}{q_i^0} \exp \left[ix \left(p_1 + p_2 - \sum_{i=1}^4 q_i \right) + D \right] \exp (2\alpha B + 2\alpha \tilde{B}) \\
& \left[\bar{\beta}_0^{(3)}(p_r^{\mathcal{R}}, q_s^{\mathcal{R}}) + \int \frac{d^3k}{k^0} e^{-ixk} \bar{\beta}_1^{(3)}(p_r^{\mathcal{R}}, q_s^{\mathcal{R}}, k) + \frac{1}{2!} \int \frac{d^3k_1}{k_1^0} \frac{d^3k_2}{k_2^0} e^{-ixk_1 - ixk_2} \bar{\beta}_2^{(3)}(p_r^{\mathcal{R}}, q_s^{\mathcal{R}}, k_1, k_2) \right. \\
& \left. + \frac{1}{3!} \int \frac{d^3k_1}{k_1^0} \frac{d^3k_2}{k_2^0} \frac{d^3k_3}{k_3^0} e^{-ixk_1 - ixk_2 - ixk_3} \bar{\beta}_3^{(3)}(p_r^{\mathcal{R}}, q_s^{\mathcal{R}}, k_1, k_2, k_3) \right],
\end{aligned} \tag{14}$$

where

$$\begin{aligned}
2\alpha \tilde{B} &= \int \frac{d^3k}{k^0} \tilde{S}_{12}(k) \theta(\sqrt{s} - k^0) \\
D &= \int \frac{d^3k}{k^0} \tilde{S}_{12}(k) \left(e^{-ixk} - \theta(\sqrt{s} - k^0) \right).
\end{aligned} \tag{15}$$

Now the dummy IR cut-off ϵ is introduced. Keeping in mind that the d^4x integral provides even stronger cut-off than $\theta(\sqrt{s} - k^0)$ and that in the small- ϵ limit $e^{-ixk} \rightarrow 1$, one can rearrange the exponents

$$\begin{aligned}
D + 2\alpha \tilde{B} &= D' + \tilde{B}(\epsilon) \\
\tilde{B}(\epsilon) &= \int \frac{d^3k}{k^0} \tilde{S}_{12}(k) \theta\left(\epsilon \frac{\sqrt{s}}{2} - k_0\right), \\
D' &= \int \frac{d^3k}{k^0} \tilde{S}_{12}(k) e^{-ixk} \theta(\sqrt{s} - k^0) \theta\left(k_0 - \epsilon \frac{\sqrt{s}}{2}\right).
\end{aligned} \tag{16}$$

After expanding the D' integral and performing d^4x integration one obtains the master formula in the familiar Monte Carlo form [12, 14, 7]:

$$\begin{aligned}
\sigma = & \sum_{n=0}^{\infty} \frac{1}{n!} \int \prod_{i=1}^4 \frac{d^3q_i}{q_i^0} \left(\prod_{i=1}^n \frac{d^3k_i}{k_i^0} \tilde{S}_{12}(k_i) \theta\left(k_i^0 - \epsilon \frac{\sqrt{s}}{2}\right) \right) \delta^{(4)}\left(p_1 + p_2 - \sum_{i=1}^4 q_i - \sum_{i=1}^n k_i\right) \\
& \exp\left(2\alpha B + \int \frac{d^3k}{k^0} \tilde{S}_{12}(k) \theta\left(\epsilon \frac{\sqrt{s}}{2} - k^0\right)\right) \left[\bar{\beta}_0^{(3)}(p_r^{\mathcal{R}}, q_s^{\mathcal{R}}) + \sum_{i=1}^n \frac{\bar{\beta}_1^{(3)}(p_r^{\mathcal{R}}, q_s^{\mathcal{R}}, k_i)}{\tilde{S}_{12}(k_i)} \right. \\
& \left. + \sum_{i>j}^n \frac{\bar{\beta}_2^{(3)}(p_r^{\mathcal{R}}, q_s^{\mathcal{R}}, k_i, k_j)}{\tilde{S}_{12}(k_i) \tilde{S}_{12}(k_j)} + \sum_{i>j>l}^n \frac{\bar{\beta}_3^{(3)}(p_r^{\mathcal{R}}, q_s^{\mathcal{R}}, k_i, k_j, k_l)}{\tilde{S}_{12}(k_i) \tilde{S}_{12}(k_j) \tilde{S}_{12}(k_l)} \right].
\end{aligned} \tag{17}$$

Reversing the above procedure we see that the *ad hoc* introduction of the real emission weight W_{ECS}^{real} of Eq. (8) into Eq. (17) amounts to the modification of the D' function:

$$D' \rightarrow D'_R = \int \frac{d^3k}{k^0} \tilde{S}_{12}(k) w^R(k) e^{-ixk} \theta(\sqrt{s} - k^0) \theta\left(k_0 - \epsilon \frac{\sqrt{s}}{2}\right). \quad (18)$$

Our goal is now to find the corresponding virtual+soft normalization weight that would *exactly* compensate for the change of normalization caused in the master formula by the replacement $D' \rightarrow D'_R$. It is evident that such a weight should have the form

$$W_{exact}^{norm} = \exp(D' - D'_R) = \exp\left(\int \frac{d^3k}{k^0} \tilde{S}_{12}(k) (1 - w^R(k)) e^{-ixk} \theta\left(k_0 - \epsilon \frac{\sqrt{s}}{2}\right)\right). \quad (19)$$

Adding and subtracting the function $\Delta U(\epsilon)$ of Eq. (10) we obtain (again in the small ϵ limit)

$$\begin{aligned} W_{exact}^{norm} &= \exp(\Delta D(\epsilon) + \Delta U(\epsilon)) \\ \Delta D(\epsilon) &= D - D_R, \\ D_R &= \int \frac{d^3k}{k^0} \tilde{S}_{12}(k) w^R(k) \left(e^{-ixk} - \theta(\sqrt{s} - k^0)\right). \end{aligned} \quad (20)$$

Let us now summarize the situation. We have constructed the *exact* compensating weight W_{exact}^{norm} . It would exactly restore the normalization of the master formula changed by the real emission weight W_{ECS}^{real} . At the same time, however, this weight would ruin the entire MC algorithm. Because of its x -dependence through the $\Delta D(\epsilon)$ function, the series of integrals over d^4x leading to four-momenta-conserving delta functions could not be performed now! Therefore we have to modify the compensating weight. We have to do it in such a way that: (1) the master formula remains independent of dummy ϵ parameter and (2) the normalization of the master formula remains as close as possible to the original normalization of Eq. (14). To fulfil these requirements we observe that the whole dependence on ϵ is contained in the $\Delta U(\epsilon)$ integral. We will not modify it and the condition (1) will be fulfilled. The trouble-making $\Delta D(\epsilon)$ function is up to the small term $(1 - w^R(k))$ identical to the original D function. As is known [15], the role of the D function is to compensate for the four-momentum non-conservation in the case of emission of multiple high energy photons. Numerically it is a very small correction, of the $\mathcal{O}(\alpha^2)$ LL type. Therefore within our accuracy we can drop this whole term and the condition (2) will be fulfilled within an $\mathcal{O}(\gamma^2)$ accuracy. Upon including the LLST correction factor $\exp\left(\left(\frac{3}{4}\right)(\bar{\gamma}_t - \gamma_s)\right)$, as described in Section 2.2, we arrive at the W_{ECS}^{norm} of Eq. (10).

B Analytical integration

We show here how to calculate analytically the $\Delta U(\epsilon)$ function of Eq. (10). In the polar variables the dk^0 integral decouples, as $\tilde{S}_{ab}(k)$ is proportional to $1/(k^0)^2$ and the ratio of

\tilde{S} functions is independent of the scale of k^0 :

$$\begin{aligned}\Delta U(\epsilon) &= \int_{\epsilon\sqrt{s}/2}^{\sqrt{s}} \frac{d^3k}{k^0} \tilde{S}_{ab}(k) (1 - w^R(k)) = - \int_{\epsilon\sqrt{s}/2}^{\sqrt{s}} \frac{dk^0}{k^0} \int d\Omega_k F(a, b, c, d; \Omega_k) = (\gamma_R - \gamma) \log \frac{\epsilon}{2} \\ \gamma_R - \gamma &= \int d\Omega_k F(a, b, c, d; \Omega_k) \\ F(a, b, c, d; \Omega_k) &= (k^0)^2 \tilde{S}_{ab}(k) \frac{\tilde{S}_{aC}(k) + \tilde{S}_{bD}(k) + \tilde{S}_{aD}(k) + \tilde{S}_{bC}(k)}{\tilde{S}_{ab}(k) + \tilde{S}_{CD}(k)}.\end{aligned}\tag{21}$$

The evaluation of $(\gamma_R - \gamma)$ simplifies if we note that this integral is Lorentz-invariant. It is easiest to show for the initial form of $\Delta U(\epsilon)$ given in Eq. (10). The only apparently Lorentz-variant part of Eq. (10) are the integration limits of k^0 . Upon a Lorentz transformation with an arbitrary parameter β , the k_0 transforms as

$$k_0 \rightarrow k_0' = \frac{k_0 - \vec{\beta}\vec{k}}{\sqrt{1 - \vec{\beta}^2}} = k_0 A(\Omega_k); \quad A(\Omega_k) = \frac{1 - |\vec{\beta}| \cos \angle(\vec{\beta}\vec{k})}{\sqrt{1 - \vec{\beta}^2}}\tag{22}$$

and the integral $\Delta U(\epsilon)$ becomes

$$\Delta U(\epsilon) = \int_{A^{-1}\epsilon\sqrt{s}/2}^{A^{-1}\sqrt{s}} \frac{d^3k'}{(k'^0)^3} F(a', b', c', d'; \Omega_{k'}).\tag{23}$$

By the rescaling transformation $k' \rightarrow Ak'$, due to the identity $\Omega_{k'} = \Omega_{Ak'}$ and the scale invariance of the function $F(a, b, c, d; \Omega_k)$, the Lorentz invariance of $\Delta U(\epsilon)$ becomes transparent.

After substituting the definition of \tilde{S} from Eq. (9) into Eq. (21), we get

$$\int d\Omega_k F(\Omega_k) = I_1 + I_2\tag{24}$$

$$I_1 = \int d\Omega_k (k^0)^2 \tilde{S}_{ab}(k) \frac{\tilde{S}_{aC}(k) + \tilde{S}_{aD}(k)}{\tilde{S}_{ab}(k) + \tilde{S}_{CD}(k)}\tag{25}$$

$$= \int d \cos \theta d\phi \frac{\alpha}{4\pi^2} \frac{2(ab)}{(n_k a)} \frac{(ac)(n_k d) - (ad)(n_k c)}{(ab)(n_k c)(n_k d) + (cd)(n_k a)(n_k b)}\tag{26}$$

$$I_2 = \int d\Omega_k (k^0)^2 \tilde{S}_{ab}(k) \frac{\tilde{S}_{bD}(k) + \tilde{S}_{bC}(k)}{\tilde{S}_{ab}(k) + \tilde{S}_{CD}(k)} = I_1(a \leftrightarrow b, c \leftrightarrow d),\tag{27}$$

where $n_k^\mu = k^\mu/k^0$. The integral contains scalar products of k with four different four-momenta a, \dots, d . With the parametrization of $(n_k u) = u^0 - u^z \cos \theta - u^x \sin \theta \cos \phi - u^y \sin \theta \sin \phi$ the $d\phi$ integral in I_1 is in principle solvable. However, in the LAB frame,

i.e. in the CMS frame of (a, b) , the $(n_k c)(n_k d)$ product in the denominator would lead to a fourth-order polynomial and its zeros would have to be found numerically. This problem can be avoided by changing the Lorentz frame to the CMS(a, c), i.e. the Breit frame of (a, c) ! The I_2 integral would similarly be evaluated in CMS(b, d) and then, due to the Lorentz invariance of the integrals I_i we can simply add $I_1(a_1, \dots, d_1) + I_2(a_2, \dots, d_2)$. One must only remember that in both integrals the a, \dots, d vectors became transformed to different values (different frames), which we indicated above as a_1, a_2 , etc.

In the CMS(a, c) we have $(n_k a) = a^0 - a \cos \theta$ and $(n_k c) = c^0 + c \cos \theta$, so that

$$I_1 = \int d \cos \theta \frac{\alpha}{2\pi^2} \frac{(ab)}{(n_k a)} \int d\phi \frac{L \cdot n_k}{M(\theta) \cdot n_k} \quad (28)$$

$$= \int d \cos \theta \frac{\alpha}{2\pi^2} \frac{(ab)}{(n_k a)} \int d\phi \frac{L^0 - L^z \cos \theta - L_x \sin \theta \cos \phi - L_y \sin \theta \sin \phi}{M^0 - M^z \cos \theta - M_x \sin \theta \cos \phi - M_y \sin \theta \sin \phi} \quad (29)$$

$$L^\mu = (ac)d^\mu - (ad)c^\mu \quad (30)$$

$$M^\mu(\theta) = (ab)(n_k c)d^\mu + (cd)(n_k a)b^\mu. \quad (31)$$

The integral over $d\phi$ can now be solved with the help of a textbook formula (cf. e.g. [20] 2.558)

$$\int_{-\pi}^{\pi} d\phi \frac{l_0 + l_1 \cos \phi + l_2 \sin \phi}{m_0 + m_1 \cos \phi + m_2 \sin \phi}$$

$$= 2\pi \frac{l_1 m_1 + l_2 m_2}{m_1^2 + m_2^2} + \frac{2\pi}{\sqrt{m_0^2 - m_1^2 - m_2^2}} \left(l_0 + \frac{l_1 m_1 + l_2 m_2}{m_1^2 + m_2^2} m_0 \right); \quad m_0^2 > m_1^2 + m_2^2 \quad (32)$$

$$= 2\pi l_0 / m_0; \quad m_1 = m_2 = 0, \quad (33)$$

to give

$$I_1 = \int d \cos \theta \frac{\alpha}{\pi} \frac{(ab)}{(n_k a)} \left(\frac{L_x M_x + L_y M_y}{M_x^2 + M_y^2} + \frac{L^0 - L^z \cos \theta - \frac{L_x M_x + L_y M_y}{M_x^2 + M_y^2} (M_0 - M_z \cos \theta)}{\sqrt{(M_0 - M_z \cos \theta)^2 - (M_x^2 + M_y^2) \sin^2 \theta}} \right). \quad (34)$$

There is one technical point related to Eq. (34), concerning the positiveness of the quantity under the square root in the last term. It is guaranteed, however, by the positiveness of the denominator $M(\theta) \cdot n_k$, which is a sum of dot products of time- and light-like four-vectors: at its minimum (with respect to ϕ) the $M(\theta) \cdot n_k$ is equal to the quantity in question. The remaining $d \cos \theta$ integral we perform numerically.

The integral I_2 is evaluated analogously to I_1 .

References

- [1] E. Migliore, 4-fermion Production at LEP2, talk given at the ICHEP 2002 Conference, Amsterdam, July 2002, to appear in the proceedings, <http://www.ichep02.nl>.
- [2] A. Pukhov *et al.*, CompHEP: A package for evaluation of Feynman diagrams and integration over multi-particle phase space, User's manual for version 33, 1999, hep-ph/9908288.
- [3] G. Montagna *et al.*, Eur. Phys. J. **C20**, 217 (2001).
- [4] F. A. Berends, C. G. Papadopoulos, and R. Pittau, Comput. Phys. Commun. **136**, 148 (2001).
- [5] Y. Kurihara *et al.*, Eur. Phys. J. **C20**, 253 (2001).
- [6] E. Accomando, A. Ballestrero and E. Maina, WPHACT 2.0: A fully massive Monte Carlo generator for four fermion physics at e^+e^- colliders, hep-ph/0204052.
- [7] S. Jadach *et al.*, Comput. Phys. Commun. **140**, 475 (2001).
- [8] M. Grünewald *et al.*, Four-fermion production in electron-positron collisions, in Ref. [21], p. 1.
- [9] S. Jadach, W. Płaczek and B. F. L. Ward, Phys. Lett. **B390**, 298 (1997).
- [10] S. Jadach, B. F. L. Ward and Z. Wąs, Comput. Phys. Commun. **130**, 260 (2000).
- [11] S. Jadach, B. F. L. Ward and Z. Wąs, Phys. Rev. **D63**, 113009 (2001).
- [12] M. Skrzypek, S. Jadach, W. Płaczek and Z. Wąs, Comput. Phys. Commun. **94**, 216 (1996).
- [13] M. Skrzypek *et al.*, Phys. Lett. **B372**, 289 (1996).
- [14] S. Jadach *et al.*, Comput. Phys. Commun. **119**, 272 (1999).
- [15] D. R. Yennie, S. Frautschi and H. Suura, Ann. Phys. (NY) **13**, 379 (1961).
- [16] E. Barberio, B. van Eijk and Z. Wąs, Comput. Phys. Commun. **66**, 115 (1991), *ibid.* **79** 291 (1994).
- [17] S. Jadach and B. F. L. Ward, Comput. Phys. Commun. **56**, 351 (1990).
- [18] G. Passarino, Nucl. Phys. **B578**, 3 (2000).
- [19] D. E. Groom *et al.*, Eur. Phys. J. **C15**, 1 (2000).
- [20] I. S. Gradshteyn, I. M. Ryzhik and A. Jeffrey, *Table of Integrals, Series and Products* (Academic Press, New York, 1994).

- [21] *Reports of the Working Groups on Precision Calculations for LEP2 Physics*, edited by S. Jadach, G. Passarino and R. Pittau (CERN 2000-009, Geneva, 2000).

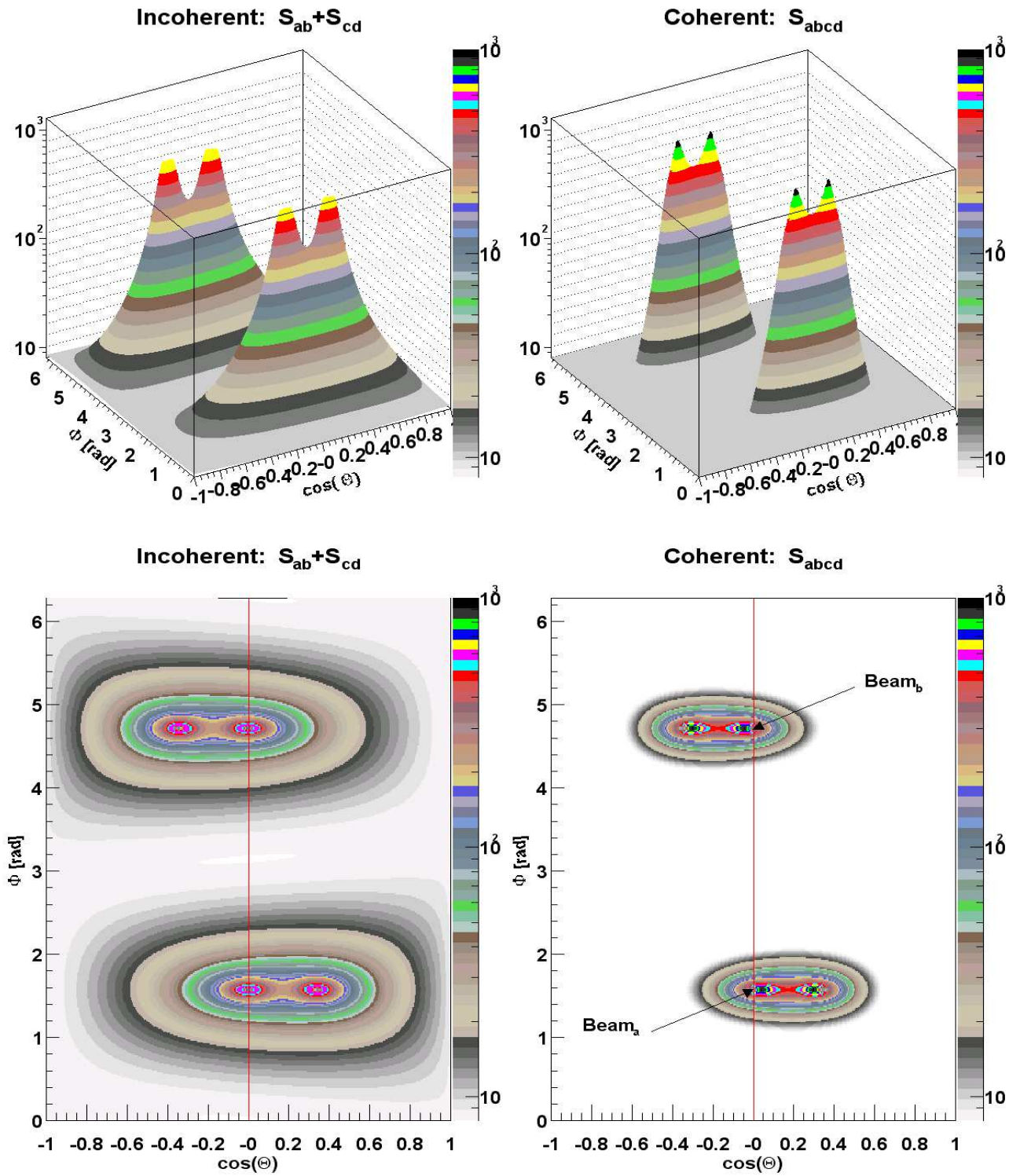


Figure 1: Photon angular distribution in "Mhamha scattering" $\mu^- \mu^+ \rightarrow \mu^- \mu^+ \gamma$ at $\sqrt{s} = 5$ GeV and muon scattering angle of 20° . The difference between left- and right-hand side plots illustrates the electric charge screening effect.

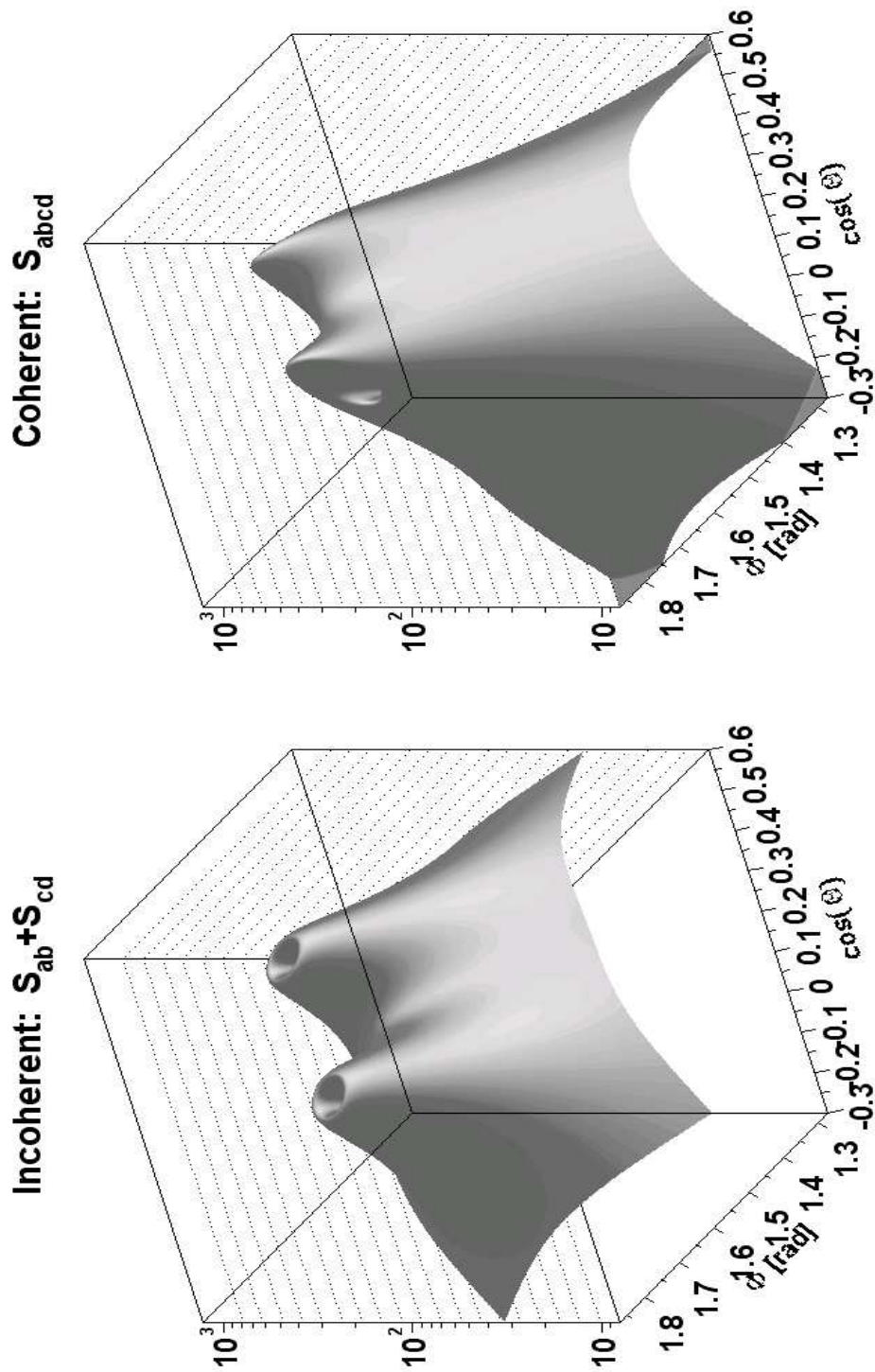


Figure 2: Photon angular distribution. The same as in Fig. 1. Range restricted to vicinity of a-c dipole. "Craters" are "helicity zeros".

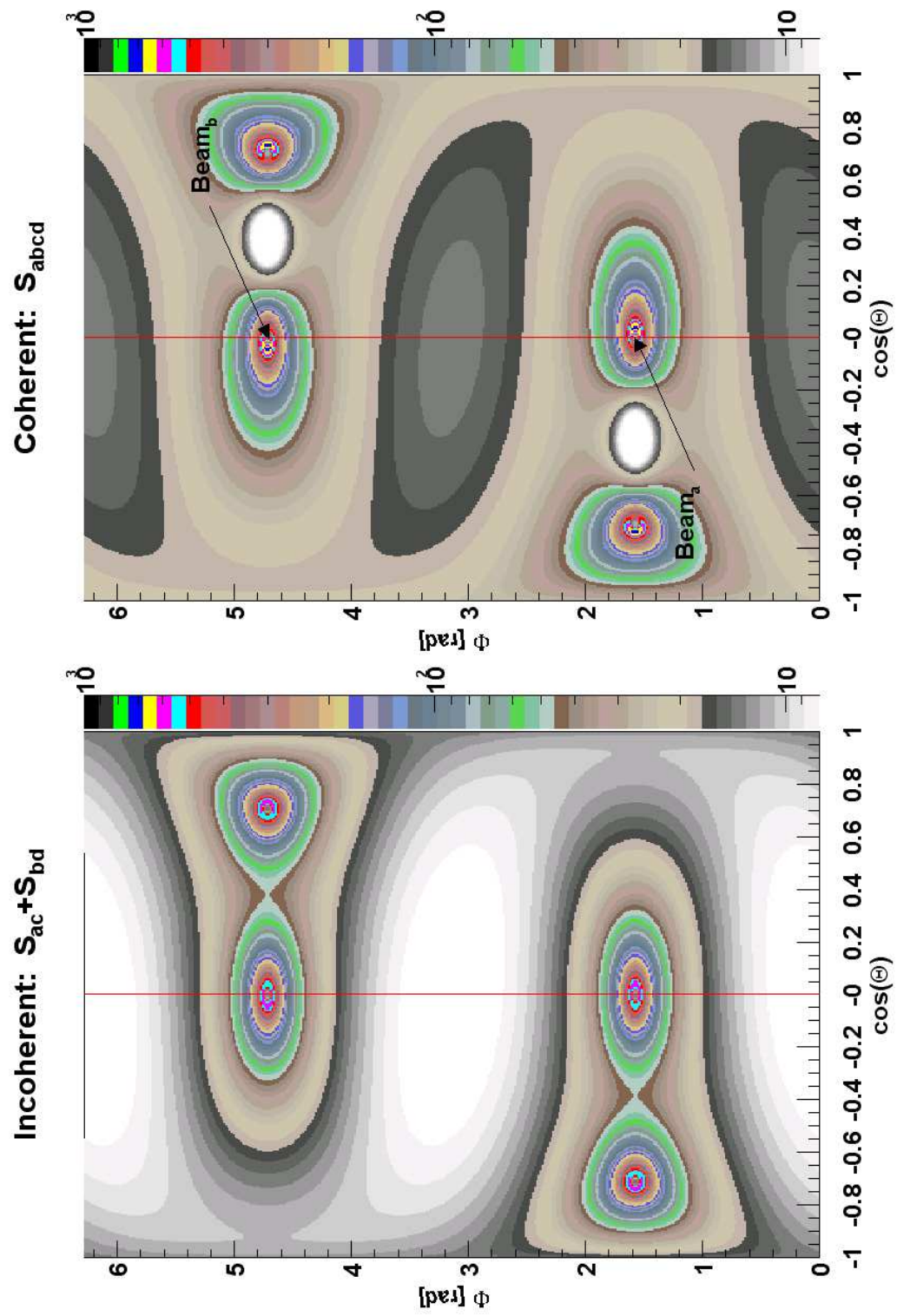


Figure 3: Photon radiation in backward scattering, $\theta = 135^\circ$.

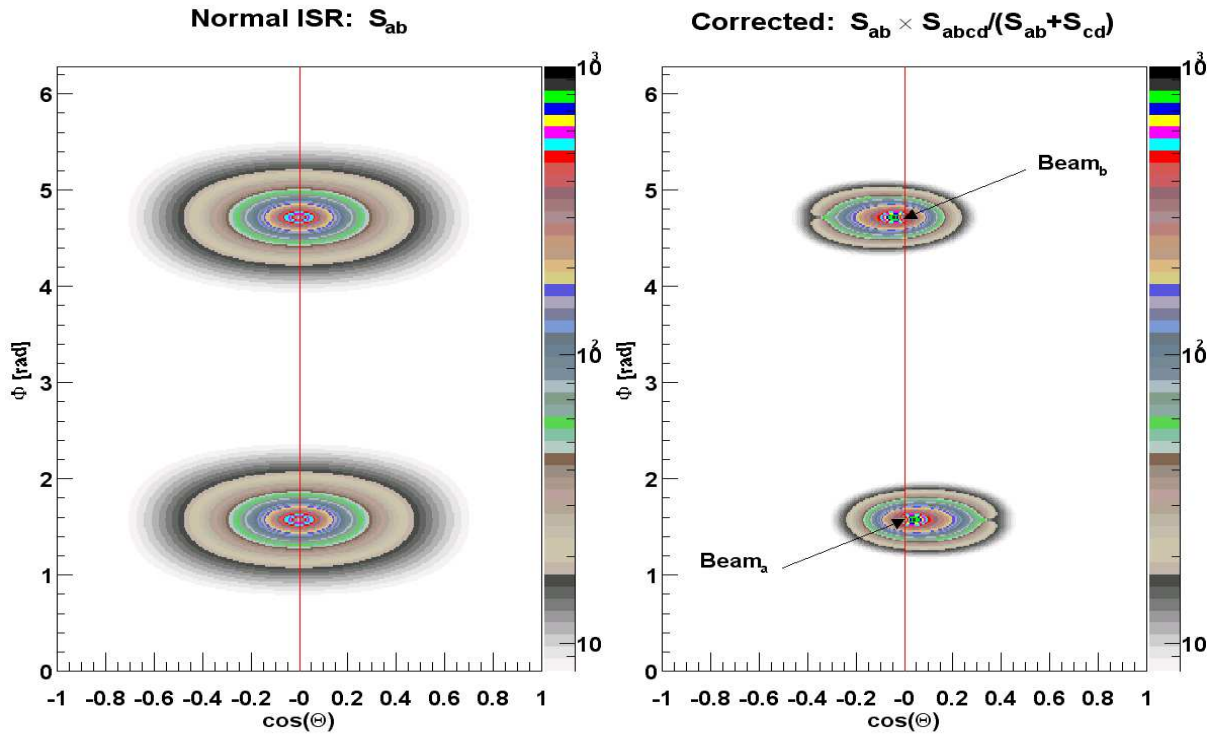


Figure 4: Photon angular distribution in “Mhamha scattering” $\mu^- \mu^+ \rightarrow \mu^- \mu^+ \gamma$ at $\sqrt{s} = 5$ GeV and muon scattering angle of 20° for the case of ISR only. The difference between left- and right-hand side plots shows the effect of the ECS correction weight.

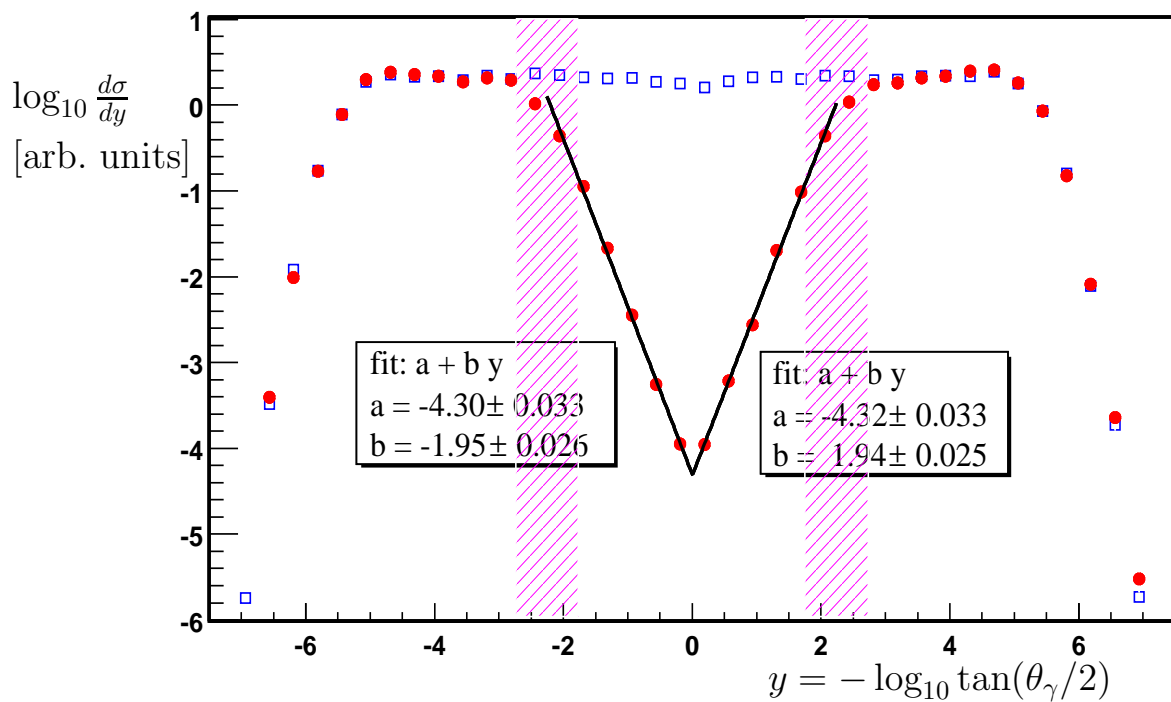


Figure 5: \log_{10} of $d\sigma/d\log_{10} \tan(\theta_\gamma/2)$ with (red dots) and without (blue open squares) the ECS correction, arbitrary units. In boxes the values of fits are shown.

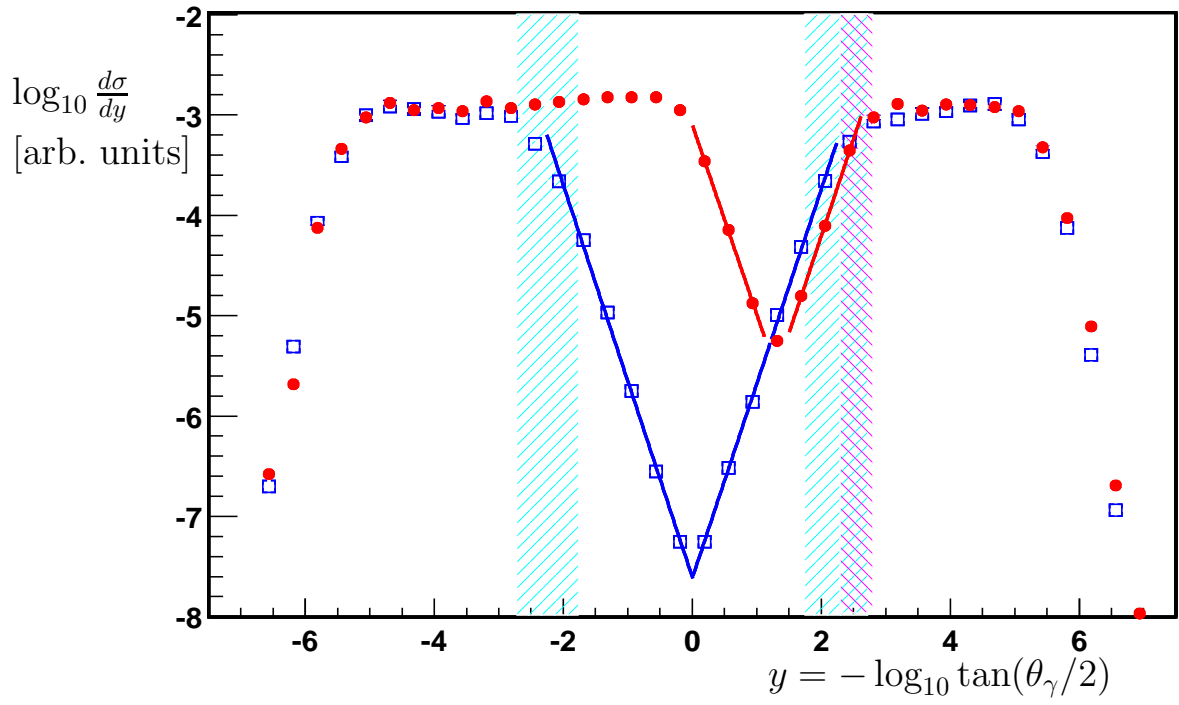


Figure 6: \log_{10} of $d\sigma/d\log_{10} \tan(\theta_\gamma/2)$ with the ECS correction for $e\nu_e u\bar{d}$ (red dots) and $e^+e^- s\bar{s}$ (blue open squares), arbitrary units.

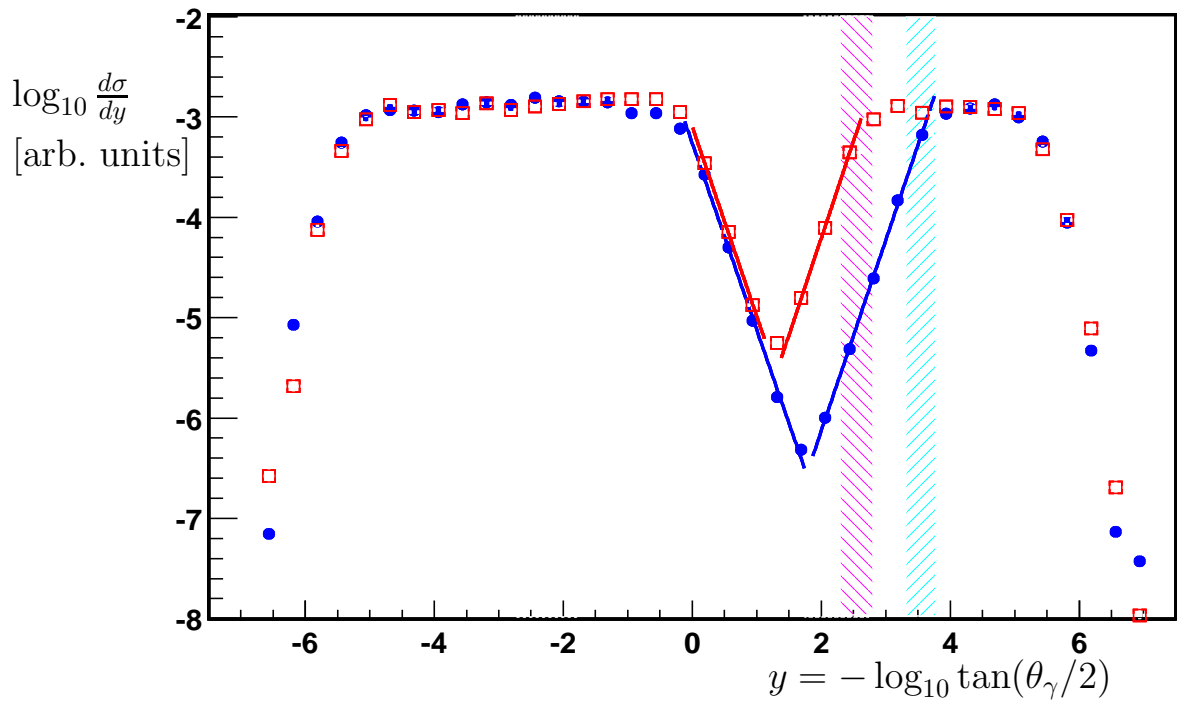


Figure 7: \log_{10} of $d\sigma/d\log_{10} \tan(\theta_\gamma/2)$ with the ECS correction for $e\nu_e u\bar{d}$ for two values of cuts for electron opening angle, arbitrary units.

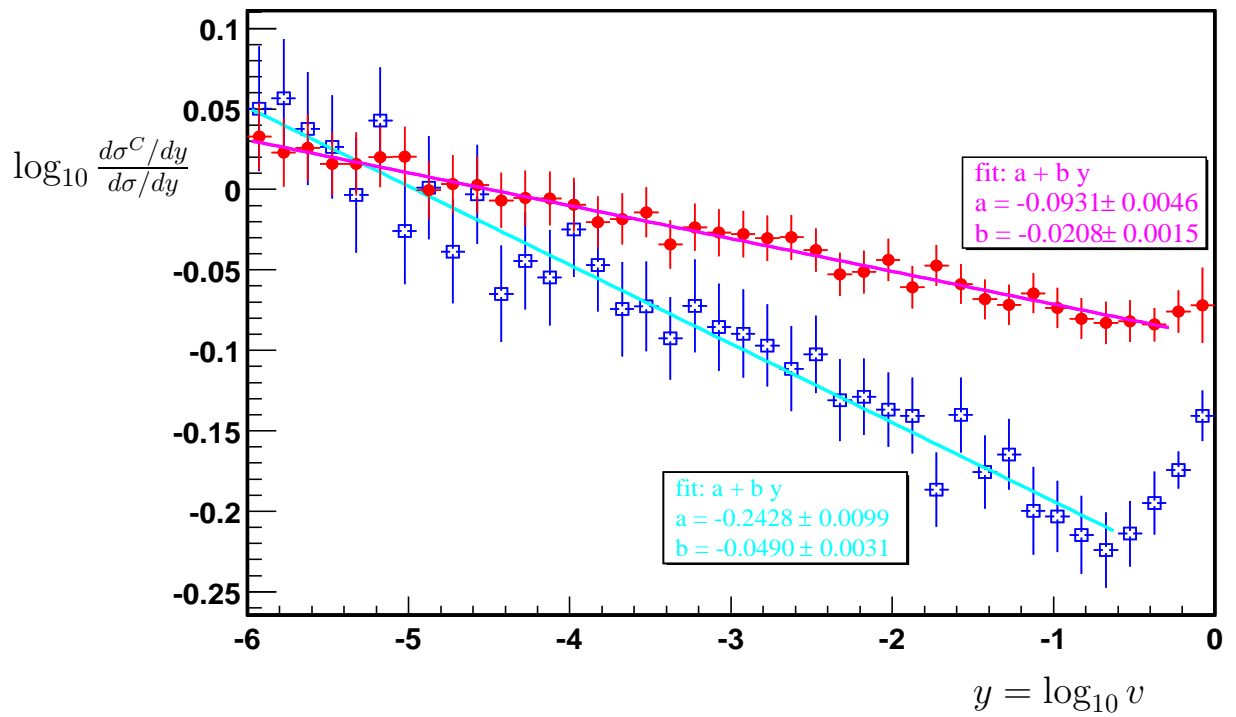


Figure 8: \log_{10} of the ratio of $(1/v)(d\sigma/d\log_{10} v)$, $v = 1 - s'/s$, with and without the ECS correction for $e\bar{\nu}_e u\bar{d}$ (red dots) and $e^+e^-s\bar{s}$ (blue open squares) final states.